

Structural and electronic properties of the Te-Si(111) surface from first principlesD. Dragoni ^{*}*Dipartimento di Scienza dei Materiali, Università di Milano-Bicocca, Via R. Cozzi 55, I-20125, Milano, Italy*

(Received 6 October 2022; accepted 1 November 2022; published 28 November 2022)

The structural and electronic properties of an atomically-flat Te-Si(111) surface have been investigated by means of density-functional theory calculations. This system is interesting because it provides a template for the epitaxial growth of inherently 2D materials. A structural model of the surface is devised that is both energetically more favorable than the ideal *on-top* model proposed in the literature and dynamically stable. The model, characterized by a staggered arrangement of Te-Te dimers in the passivation layer, is a semiconductor with a narrow band gap resulting from the misalignment of the Te₂ units. As for the *on-top* case, however, this structure does not fully conform to the available experimental observations. A finite-temperature model is hence prepared by means of molecular dynamics simulations at 300 K. It turns out that such a model is characterized by a disordered passivation layer consisting of randomly oriented Te₂ units and Te chains, which makes it effectively compliant with all the experimental structural data at hand. In addition, it is also a narrow-gap semiconductor compatible with the electrical conductance measurements. These findings suggest that this model is a good candidate for representing the Te-Si(111) surface.

DOI: [10.1103/PhysRevB.106.195427](https://doi.org/10.1103/PhysRevB.106.195427)**I. INTRODUCTION**

In the last decade, two-dimensional (2D) materials have attracted a renewed scientific attention due to their exceptional properties that might potentially revolutionize the fields of optoelectronics [1,2], thin film transistors [3], quantum information [4,5], and low-power spintronic [6]. Beyond graphene [7] (or its functionalized counterparts [8]) and boron-nitride [9], excellent examples of such materials are mono-elemental group IV and group V single-layered compounds [10,11]. Similarly, are the transition metal carbonitrides (MXenes) [12]. Another vast class of inherently 2D materials, consisting of weakly bonded blocks of a few atomic layers, is constituted by chalcogenide compounds such as transition-metal dichalcogenides [13], V₂-VI₃ chalcogenides including topologically-nontrivial Bi₂Te₃, Sb₂Te₃, Bi₂Se₃ [14], and (GeTe)_n-(Sb₂Te₃)_m (GST) alloys. The latter are of great relevance for next-generation phase change memory applications [15–17].

A well-established methodology for growing high-quality single layer/block thin films, as well as heterostructures of such 2D materials is van der Waals (vdW) epitaxy [18,19]. Within this framework, the Si(111) substrate is a common practical choice that easily provides extended atomically flat growing templates ideal for the integration of 2D materials with Si microelectronics. This substrate is typically terminated with a passivation layer of atomic thickness in order to saturate the dangling bonds that would otherwise induce surface reconstructions [20,21]. The choice of the passivating

species, however, is known to affect the morphology and crystallinity of the epitaxially grown samples [22]. The simplest passivation is attained by means of hydrogen atoms, which interact with the deposited 2D material essentially via weak van der Waals forces. This chemical decoupling at the substrate-material interface enables heteroepitaxial growth even in the case of very large in-plane lattice mismatch between the grown material and the substrate. On the other hand, however, it can also be responsible for poor adhesion [23], inducing the formation of randomly oriented rotational domains during the growing process, which ultimately cause a polycrystalline sample morphology [22]. To alleviate this issue, hydrogen atoms are typically replaced by other atomic species that exhibit a partial, not purely van der Waals, coupling with the atoms of the deposited material.

Antimony, for example, has been successfully used for growing high quality Sb_{2+x}Te₃ [22,24] and GST [25] films, or GeTe-Sb₂Te₃ superlattices [26] by molecular beam epitaxy (MBE).

The Te passivation has also been considered for the epitaxial growth of the aforementioned compounds and has been actually used for growing topological insulator Bi₂Te₃ films [27,28]. At variance with the Sb-Si(111) case [29,30], however, the structural and electronic properties of the Te-Si(111) substrate have only recently been investigated [28]. The authors of Ref. [28] showed through a combined analysis based on scanning transmission electron microscopy (STEM), scanning tunneling microscopy (STM), and low-energy electron diffraction (LEED), that the Te passivation of an unreconstructed Si(111) substrate results in a stable Te-Si(111)-(1 × 1) reconstruction, with an average out-of-plane distance of the Te atoms from the underlying Si bilayer of 2.88 Å. In the same paper, it is proposed to model such a reconstruction by means of an ordered passivation layer model, here referred to as

^{*}Present address: Leonardo S. p. A., Piazza Monte Grappa 4, 00195, Roma, Italy; daniele.dragoni.ext@leonardo.com

on-top model, where all Te atoms stay atop the exposed Si atoms of the substrate (T1 site). Density-functional theory (DFT) calculations showed in fact that the T1 positioning of the ordered Te layer relative to the substrate is energetically more favored as compared to other positions and that the theoretical average distance between the Te layer and the topmost Si(111) bilayer of the model is in excellent agreement with experimental observations. Conversely, the electronic structure of such a model, which is predicted as metallic, is shown to be in stark contrast with the very low surface conductance highlighted by *in situ* electrical transport measurements, which is three orders of magnitude smaller than the one typically associated to topological surface states. This apparent contradiction was partially motivated by means of the low Fermi velocity of the states, which contributes the most to the calculated density of states (DOS) at the Fermi level and eventually invoking a high surface roughness of the prepared Si substrate.

In this paper, an alternative disordered model for the Te-Si(111) substrate is proposed as an attempt to fully reconcile theory and experimental observations of Ref. [28] without the need to invoke surface roughness. The new model is developed through intermediate steps, starting from the ordered *on-top* model proposed above, using DFT calculations and physical intuition.

II. COMPUTATIONAL DETAILS

Density-functional theory simulations have been performed by means of the Quantum Espresso suite of programs [31], using norm-conserving Troullier-Martins pseudopotentials [32] with the PBE xc-functional [33]. The semi-empirical D2 correction by Grimme [34] is also used to account for van der Waals interactions. The Kohn-Sham orbitals are expanded in a plane wave basis set with an energy cutoff of 24 Ry, while Brillouin zone integration for the different structures is achieved using various Monkhorst-Pack [35] grids with a maximal k point linear spacing of 0.15 (0.1) \AA^{-1} along the in-plane (out-of-plane) reciprocal cell vectors, along with a Marzari-Vanderbilt smearing [36] of 0.08 Ry. *Ab initio* Born-Oppenheimer molecular dynamics (MD) runs are carried out within a constant-volume constant-temperature (NVT) ensemble with a time step of 4 fs, controlling the temperature by means of a Berendsen thermostat [37] with a characteristic relaxation time equivalent to 10 time steps. A reduced energy cutoff of 20 Ry has been used along with a special $(1/4, 1/4, 1/4)$ point sampling for computational efficiency.

The Si(111) substrate is modeled through a slab geometry with periodic boundary conditions (PBC). Each slab, taken parallel to the xy plane of the system of reference, consists of five atomic double layers stacked along z , and is separated by its periodic images by 20 \AA vacuum regions to minimize spurious interactions. The top and bottom Si(111) surfaces are terminated by tellurium and hydrogen atoms respectively. Different simulation cells are considered that are $n \times m$ in-plane repetitions of a reference hexagonal unit cell containing 12 atoms in total (10 Si, 1 H, 1 Te). The hexagonal in-plane lattice parameter is $a_h \equiv a_c/\sqrt{2} = 3.840 \text{ \AA}$, with $a_c = 5.431 \text{ \AA}$ being the experimental cubic lattice parameter of silicon crystal at room temperature [38,39]. Available

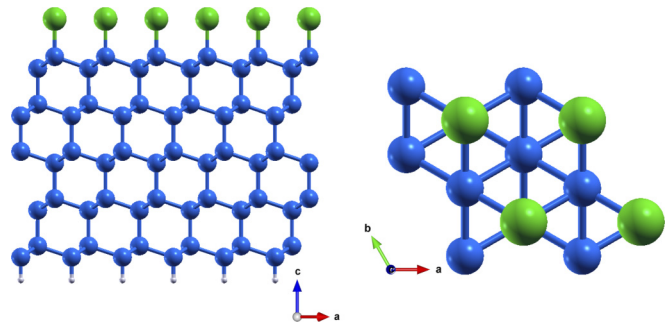


FIG. 1. Equilibrium structure of the Te-Si(111)- (1×1) substrate reconstruction with *on-top* passivation of Te atoms as proposed in Ref. [28]. The structure is represented by means of a 2×2 supercell. (a) Side and (b) top view are reported.

GGA-PBE calculations without van der Waals corrections are known to overestimate such experimental value by 0.7% [40]. In the attempt to mimic a semi-infinite substrate configuration, all simulations are carried out freezing the five Si atomic layers closest to the H-terminated surface at their equilibrium positions in the crystal bulk. The H atoms are also frozen at the ideal T1 sites at their theoretical equilibrium distance from the Si substrate. For computational reasons, the MD runs are carried out using thinner slabs of six Si atoms rather than 10. In this case, only the three Si layers closest to the H-passivated surface are kept frozen.

III. RESULTS AND DISCUSSION

As a starting point of the study, in the attempt to provide a model for the Te-Si(111) surface, which fully reconciles theory and experimental data, it is convenient to examine in detail the ordered *on-top* picture proposed in Ref. [28]. Within this model, all Te atoms are equivalent by symmetry and form a perfect in-plane hexagonal lattice at nonbonding Te-Te distances [41–43]. At the same time, each Te atom at T1 position forms a σ bond with the corresponding Si atom underneath, thus saturating all the dangling bonds at the Si(111) surface (see Fig. 1). Onefold coordination is, however, quite unusual for Te atoms, which rather have a known preference for divalency and twofold coordination [44]. This can be observed, for example, in the crystalline and amorphous phases of elemental Te [41,44]. In these systems, such a coordination ensures an effective filling of the electronic outer shell, which entails the opening of a relatively small band gap E_g in the respective electronic band structures, as reported by magnetoabsorption measurements for crystal samples ($E_g = 0.335 \text{ eV}$) [45] and by first-principles calculations for crystal/amorphous models ($E_g = 0.4/0.32 \text{ eV}$) [41]. Conversely, in the *on-top* model, onefold coordination results in an open shell configuration, which originates the observed metallic behavior in a band structure picture [see also top panel of Fig. 1(a)]. In fact, out of the four $5p$ valence electrons that govern the chemical reactivity of this element (the $5s$ valence electrons occupy deep energy levels and are therefore chemically unreactive [46,47]), one is involved in the formation of the Si-Te bond, while the other three partially occupy the manifold of orthogonal $p_{x,y}$ states.

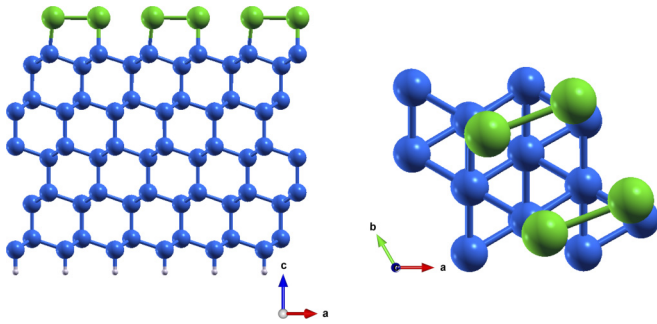


FIG. 2. Equilibrium structure of the dimerized (2×1) reconstruction of the Te-Si(111) substrate. The Te dimers are all aligned in the same direction. The structure is represented by means of a 2×2 (1×1) supercell. (a) Side and (b) top view are reported.

Despite these arguments, the structural properties of this ordered model are reported to be in excellent agreement with the experimental observations. One could hence try to devise alternative models, which preserve as much as possible the correspondence with the structural, experimentally observed features, yet restoring a more customary twofold coordination for Te atoms. In this paper, this is attained by introducing tailored modifications to the original ordered *on-top* model, which entail the relaxation of the ideal hexagonal symmetry of the Te layer. Various models have then been developed following this line of reasoning that are presented in the following sections.

A. Tellurium dimerization

The first and easiest model considered here is characterized by an in-plane arrangement where Te atoms are paired up to form Te_2 units all aligned in the same direction, as visible in Fig. 2. This model actually corresponds to a (2×1) reconstruction, at variance with the experimental evidences, but it is nevertheless instructive to be analyzed in order to verify the initial hypothesis that twofold coordination might induce an insulating surface character through the opening of an electronic band gap at the Fermi level. The equilibrium structure of the model is obtained through a structural relaxation of a 2×1 supercell with the apical Te atoms initially displaced from the ideal T1 sites in a random fashion. Different random displacements are actually taken into consideration. For small initial displacements the ideal *on-top* configuration is always recovered. Conversely, for large enough displacements, the system is observed to relax to the new dimerized configuration that is approximately 5 meV/at lower in energy than the undistorted model. The Te_2 dimers are slightly twisted relative to the high symmetry directions defined by the underlying hexagonal Si-lattice thus to adjust the Te-Te distance to an optimal value $d_{\text{Te}_2} = 3.22 \text{ \AA}$. This value lays in between the experimental intrachain and interchain distances found in crystalline Te [48], and is compatible with the theoretical Te-Te coordination distance reported for melt-quenched amorphous models of Te [41] and Te rich In_2Te_5 [43] at room temperature. At the same time, the Te-Te distance is slightly larger than the cutoff distance $r_{\text{cut}} = 3.1 \text{ \AA}$ for the formation of a covalent Te-Te bond suggested by the analysis

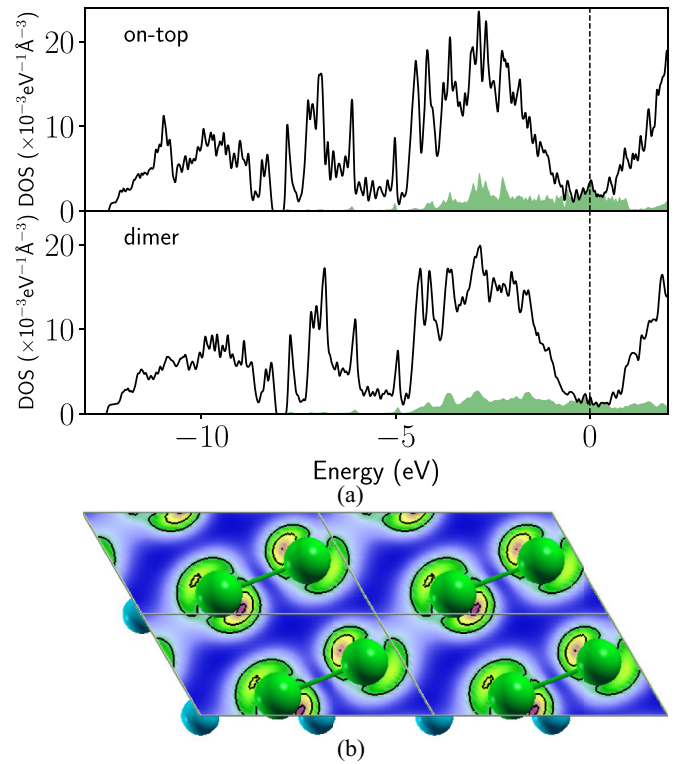


FIG. 3. (a) Density of states calculated for the (upper panel) *on-top* and (lower panel) dimer-aligned models. The projected DOS on the Te p states is highlighted by the shaded area. The Fermi energy is set to zero. The DOS is broadened with Gaussian functions 21-meV wide. (b) Local DOS of dimer-aligned model integrated in the energy range $(-75, +10 \text{ meV})$ about the E_F and projected onto the plane of Te atoms. The data are represented by means of a 4×2 (1×1) supercell for the sake of clarity.

of the electron-localization function (ELF) and Wannier centers in $\text{Ge}_2\text{Sb}_2\text{Te}_5$ [42]. For this model, the calculated ELF (see Fig. S1 in the Supplemental Material, SM, [49]) takes values marginally larger than 0.5 along the entire connectivity segment of the Te_2 unit, which would support the presence of a weak chemical bond in between the Te_2 atoms. At the same time, the ELF analysis also discards the presence of chemical bonds in between atoms of adjacent Te_2 units, which are 3.5 \AA apart. As in the ideal model, each tellurium remains bonded to the Si atom underneath, with an average distance between the Te layer and the underlying Si bilayer of $d_{\text{Te-Si}_2} = 2.82 \text{ \AA}$. This value is only 0.05 \AA smaller than the one computed for the *on-top* case, and still in agreement with the experimental data of 2.88 \AA [28].

Contrary to what originally expected, the analysis of the electronic properties still highlights a metallic character. The value of the DOS [50] at the Fermi level E_F , albeit reduced with respect to that of the *on-top* model, is in fact finite [see bottom panel of Fig. 3(a)]. The projected density of states (pDOS) clearly attributes this finite value to the (in-plane) $p_{x,y}$ states of tellurium. At the same time, the projection of the DOS integrated in the energy range $[-75, +10 \text{ meV}]$ about E_F onto the tellurium plane suggests that metallicity is imputable to nonbonding π -like states, which result from a in-plane superposition of lone pairs belonging to neighboring Te atoms

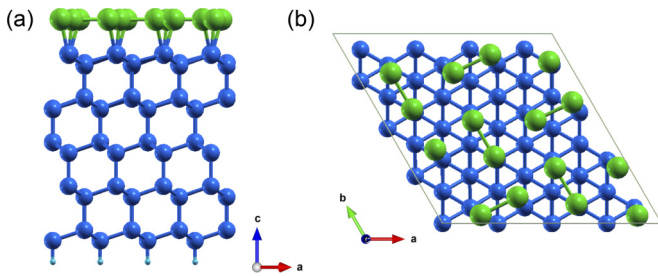


FIG. 4. (a) Side and (b) top view of a fully relaxed model for a Te-Si(111) surface with staggered Te_2 covering in a $4 \times 4 (1 \times 1)$ supercell.

in adjacent aligned dimers [see Fig. 3(b)]. The alignment of Te_2 dimers hence appears to favor a metallic character.

B. Dimers misalignment and band gap opening

An interesting question that the latter observation poses is whether the reverse is also valid, i.e., whether the misalignment of Te_2 units could provide a route to suppress surface metallicity. To validate this conjecture, it would be useful to investigate the electronic properties of ordered models that maximize the in-plane misalignment of the Te units introduced above. One possible realization of such models is provided by the 4×4 staggered configuration schematically represented in Fig. S2 of the SM [49]. Within the ideal staggered structure, the dimers are all oriented along the high symmetry directions of the hexagonal lattice defined by the unreconstructed Si(111)-(1 \times 1) substrate. The relaxation of this structure yields to the equilibrium configuration reported in Fig. 4, which features a total energy 11.3 meV/at lower than that of the model with aligned Te_2 units.

From a structural point of view, it is possible to note that after the relaxation half of the Te_2 units are oriented along the **b** vector of the supercell and the other half oriented approximately along the orthogonal direction. The average Te-Te distance within the Te_2 units is $d_{\text{Te}_2} = 2.92 \text{ \AA}$, rather smaller than the same quantity of the previous model. This value is comparable to the intrachain distance measured in crystalline Te [48], close to the most probable Te-Te connectivity distance in amorphous models of Te [41] and Te rich In_2Te_5 [43] at 300 K, and smaller than the cutoff distance for the formation of a covalent Te-Te bond found in Ref. [42]. The average distance between the top Te layer and the center of mass of the underlying Si bilayer is $d_{\text{Te-Si}_2} = 2.83 \text{ \AA}$, once again in agreement with the experimental value of 2.88 \AA [28]. It is also worth to mention that the model is dynamically stable as observed from the analysis of a MD trajectory carried out at 300 K for a few picoseconds.

As for the previous model, the ELF analysis supports the presence of a chemical bond in between the atoms involved in the dimers (see Fig. S3 in the SM [49]) while excluding a bonding state in between atoms of adjacent Te_2 units.

On the other hand, at variance with the previous model, the calculated band structure highlights a semiconductive character with a narrow direct band gap of 0.29 eV (see Fig. 5). This value is similar to the theoretical band gaps in the crystalline and melt-quenched amorphous phases [41]. As

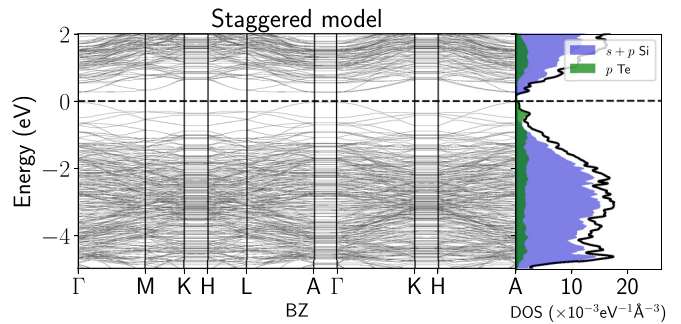


FIG. 5. Band structure (left panel) and density of states (right panel) calculated for the staggered model. The DOS is broadened with Gaussian functions 21-meV wide. The VBM energy is set to zero. A direct energy band gap of 0.29 eV is found.

clearly shown by the projected density of states, the valence band maximum (VBM) can be ascribed to p states of Te atoms, whereas the conduction band minimum (CBM) is mainly attributable to Si states. At the same time, the energy gap between the highest occupied and lowest empty surface p -Te states is 0.57 eV, i.e., almost twice as large as the actual band gap. This might suggest that the most relevant channels for conductivity would not be confined within the atomically thin passivating layer. Moreover, these findings demonstrate that surface metallicity can be suppressed by the misalignment of Te_2 units through lone-pairs misalignment. Additionally, these highlight also a direct connection between structural and electronic properties that might serve to rationalize the origin of the metal-semiconductor transition in 3D Te based compounds.

Thanks to its semiconducting behavior, the model is expected to display an electric conductivity that is orders of magnitude lower than that of a metallic system, which better conforms to the experimental evidences of Ref. [28]. It would be tempting to consider this model as a good candidate for describing the ground state Te-Si(111) substrate. As a matter of fact, however, its supercell periodicity is still not fully compatible with the observed unreconstructed Si(111)-(1 \times 1) LEED pattern.

C. Locally disordered model

The models considered so far are all enclosed in an energy range smaller than 25 meV/at. Hence, it is reasonable to suppose that, from a structural perspective, the passivation layer of an experimentally prepared Te-Si(111) surface at room temperature might realistically consist of a superposition of different Te arrangements. Within this picture, the Te-Si(111) substrate could be effectively described as a locally disordered *on-top* model, where the Te atoms are displaced (on average) from the ideal T1 site to form Te dimers with random in-plane orientation.

Such a model is expected to originate a surface diffraction pattern that is qualitatively compatible with the (1 \times 1) reconstruction observed in LEED measurements [28]. Two scenarios are in fact possible. In the first one, the long-range order of the ideal *on-top* model is retained on average (up to a certain degree). Deviations from the ideal long-range

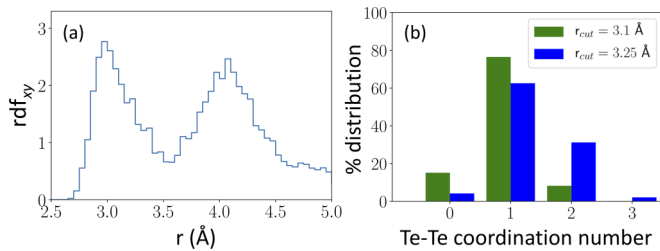


FIG. 6. (a) In-plane radial distribution function of Te atoms at 300 K. (b) Distribution of coordination numbers of Te atoms with other Te atoms within the passivation layer using two different cutoff values as reported in the legend.

order would therefore affect the diffraction pattern only from a quantitative point of view [51], by reducing the integer-order beam intensities of the ideal hexagonal pattern, and/or enhancing the diffusive background [52]. In the second scenario, instead, the degree of disorder is such that coherency of the electrons scattered within this layer is lost. Even in this case, however, a constructive diffraction signal compatible with that of a (1×1) reconstruction would be built by the electrons coherently diffracted by the first Si layers of the substrate, which typically contribute to the formation of LEED pattern due to the finite penetration of length of the incident beam.

In order to better characterize the properties of the Te-Si(111) surface at room temperature, a 6×6 supercell model was prepared where local disorder is introduced by means of successive MD simulations carried out in a canonical ensemble at different temperatures. The starting point of this set of simulations is the model with aligned dimers presented above, which is initially evolved in time for 2 ps at 600 K to loose memory of the initial condition and to randomize the Te positions. During this part of trajectory, the Te atoms undergo indeed large oscillations about the T1 site of reference, with the repeated formation and breaking of in-plane Te_2 pairs. No breaking event of Si-Te bonds is observed. An instantaneous quenching at 300 K is then performed, followed by an annealing run of further 6 ps. At this temperature, the Te atoms exhibit small oscillations around equilibrium positions that are mostly displaced from the T1 sites. Occasional local reconfigurations are also observed in the time of the simulation. Detailed information on the structural properties of the passivation layer of the model are conveyed by the Te-Te radial distribution function averaged over the last 3 ps of the trajectory. As visible from Fig. 6(a), this features a first maximum at 2.95 Å and a second one at 4.1 Å respectively, which correspond to bonding and nonbonding distances of Te atoms on neighboring T1 sites. Despite a first minimum is visible at 3.5 Å, the distribution of Te-Te coordination number is calculated adopting a hard connectivity cutoff of 3.1 Å and 3.25 Å as suggested in Ref. [42] and Ref. [43] for amorphous GST and In_2Te_5 at 300 K in Ref. [43] [see Figs. 6(b)]. In both cases it can be observed that Te atoms are mainly onefold coordinated with other Te atoms, while only a minority of them are zero- or twofold coordinated. Hence, the majority of Te atoms form dimers, which appear as misaligned with each other by visual inspection. The fact that the Te dimers have survived the high-temperature/quenching

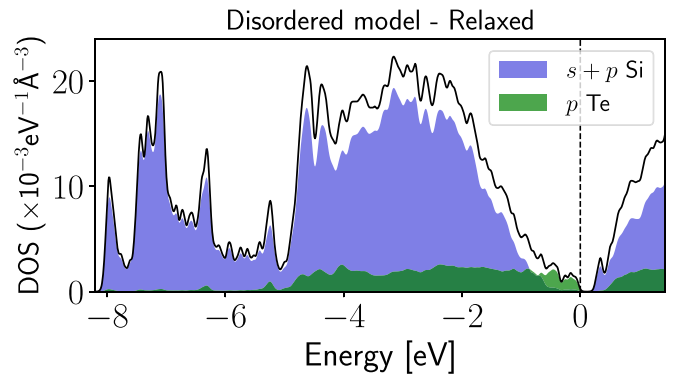


FIG. 7. Density of states (right panel) calculated for the relaxed disordered model. The DOS projections of the p states of Te atoms and of the $p + s$ states of Si atoms are highlighted by the colored areas. The DOS is broadened with Gaussian functions 21-meV wide. The VMB energy is set to zero.

treatment, reinforces *a posteriori* the idea that these units are naturally present at room temperature.

In the attempt to further characterize the structure of the model, the mean and standard deviation of the distribution of in-plane displacements of the Te atoms relative to the ideal hexagonal site of reference are then calculated by averaging over time and sites. As expected for a locally disordered system, the mean estimator corresponds approximately to the zero vector. The effective standard deviation (calculated as the average of the standard deviations along the x and y axes) is instead 0.45 Å, i.e., $\approx 0.12 a_h$. This rather large value, relative to the typical thermal displacements in bulk systems amounting to a few percent of the lattice parameter [53], casts doubts on whether the passivation layer can generate a constructive diffraction signal, which would contribute to the overall LEED pattern.

The average distance $d_{\text{Te-Si}_2} = 2.82$ Å between the Te layer and the Si bilayer is compatible with the experimental data, although slightly lower than that of the ordered models.

The last snapshot of the trajectory is eventually relaxed and considered for further analysis. Its final energy is only 2 meV/at higher (i.e., essentially degenerate within the DFT error) than the 4×4 staggered model, which once again supports the idea that local disorder can be easily observed in Te-Si(111) substrates. The structure of the relaxed configuration, reported in Fig. S3 in the SM [49], displays characteristics, which conform to those extracted from the analysis of the trajectory at 300 K. If a connectivity cutoff of 3.1 Å is used, the majority of Te atoms are involved in the formation of dimers with no preferential in-plane orientation. Some atoms are zero coordinated, while others are two-fold coordinated, forming trimers or chains containing up to 7 atoms. The ELF analysis (see Fig. S3 in the SM [49]) highlights a partial localization of electrons, interpreted as the signature of a weak covalent bond, along the connectivity segments. The ELF also remains only slightly larger than 0.5 in between atoms up to 3.25 Å apart.

As expected, the calculated DOS and band structure (see Fig. 7) indicate a semiconducting character, with a narrow electronic band gap of ≈ 0.3 eV. A similar behavior is also observed for the unrelaxed configuration (see Fig. S4 in SM

[49]). Albeit not directly computed, the average in-plane electrical dc conductivity is then expected to be orders of magnitude smaller than the one associated with the metallic *on-top* model. This result complies with the experimental measurements of a surface conductance that is three orders of magnitude smaller than typical values measured for topological insulators [28].

IV. CONCLUSIONS

The structural and electronic properties of an atomically flat Te-Si(111) surface have been investigated by means of density-functional theory calculations. Various structural models are discussed that correspond to tailored modifications of the ordered *on-top* model proposed in Ref. [28].

Firstly, it is shown that the total energy of the system decreases when Te atoms of the ideal *on-top* model are allowed to (i) shift from their reference T1 sites and (ii) to pair off in dimers lying in the surface plane. When such dimers are all equally oriented and aligned as in a (2×1) reconstruction, the calculated DOS displays a finite value at the Fermi level, with the largest contribution given by nonbonding π -like states originated by the superposition of lone pairs in adjacent aligned Te₂ units. Conversely, it is shown that is possible to open up a narrow electronic band gap through the disalignment of lone pairs, as observed in the case of a paradigmatic 4×4 staggered surface model. The mechanism of alignment-misalignment of the lone pairs, which correlates with the alignment-misalignment of the Te₂ units, is therefore identified as a control parameter of the metallic-to-semiconductor transition. The staggered model is also shown to have the lowest energy among those considered in this paper and to be dynamically stable at 300 K. At the same time, its surface periodicity is not fully compatible with the LEED measurements reported in Ref. [28].

Based on the energetics of the various analyzed structures (spread < 25 meV/at), it is then suggested that the Te-Si(111)

surface at room temperature can be modelled as a statistical mixture of a variety of ordered models that differ by the arrangement of the Te atoms about the T1 ideal sites. A finite temperature model is hence prepared by means of DFT molecular dynamics simulations carried out with a 6×6 supercell annealed at 600 K and then quenched to 300 K. The analysis of its structural properties reveals the tendency of Te atoms to stay either in one- or twofold in-plane coordination, forming misaligned and randomly-oriented Te₂ units or chains, which are interpreted as defective aggregations of Te₂ units. Also, the total energy of the relaxed model is found only 2 meV higher than the staggered case. Overall, these findings validate the picture that the Te-Si(111) surface is actually constituted by a locally disordered passivation layer that breaks the perfect hexagonal symmetry of the ideal *on-top* model, resulting nevertheless in a structure that is effectively compatible with the experimental LEED diffraction measurements. At the same time, both the relaxed and unrelaxed disordered models display a semiconducting character with an electronic band gap of 0.29 eV.

In conclusion, the locally disordered model is shown to conform to all the experimental data at hand, thus providing a reliable atomic-scale representation of the Te-Si(111) surface capable to reconcile theory and experiments.

ACKNOWLEDGMENTS

It is a pleasure to thank M. Bernasconi, D. Brunetti, S. Cecchi, and D. Ceresoli for fruitful and insightful discussions. The author also acknowledges M. Bernasconi and D. Brunetti for critical reading the manuscript, and the computational resources provided by the ISCRA program at Cineca (Casalecchio di Reno, Italy). This work was partially funded by the European Union's Horizon 2020 research and innovation programme under Grant Agreement No. 824957 (BeforeHand: Boosting Performance of Phase Change Devices by Hetero- and Nanostructure Material Design).

-
- [1] Q. H. Wang, K. Kalantar-Zadeh, A. Kis, J. N. Coleman, and M. S. Strano, *Nat. Nanotechnol.* **7**, 699 (2012).
 - [2] A. C. Ferrari, F. Bonaccorso, V. Fal'ko, K. S. Novoselov, S. Roche, P. Bøggild, S. Borini, F. H. Koppens, V. Palermo, N. Pugno *et al.*, *Nanoscale* **7**, 4598 (2015).
 - [3] G. Fiori, F. Bonaccorso, G. Iannaccone, T. Palacios, D. Neumaier, A. Seabaugh, S. K. Banerjee, and L. Colombo, *Nat. Nanotechnol.* **9**, 768 (2014).
 - [4] P. Recher and B. Trauzettel, *Nanotechnology* **21**, 302001 (2010).
 - [5] X. Liu and M. Hersam, *Nat. Rev. Mater.* **4**, 669 (2019).
 - [6] J. E. Moore, *Nature (London)* **464**, 194 (2010).
 - [7] A. K. Geim and K. S. Novoselov, in *Nanoscience and Technology: A Collection of Reviews from Nature Journals* (World Scientific, Singapore, 2010), pp. 11–19.
 - [8] V. Georgakilas, M. Otyepka, A. B. Bourlinos, V. Chandra, N. Kim, K. C. Kemp, P. Hobza, R. Zboril, and K. S. Kim, *Chem. Rev.* **112**, 6156 (2012).
 - [9] Y. Lin and J. W. Connell, *Nanoscale* **4**, 6908 (2012).
 - [10] S. Cahangirov, M. Topsakal, E. Aktürk, H. Şahin, and S. Ciraci, *Phys. Rev. Lett.* **102**, 236804 (2009).
 - [11] M. Pumera and Z. Sofer, *Adv. Mater.* **29**, 1605299 (2017).
 - [12] M. Naguib, V. N. Mochalin, M. W. Barsoum, and Y. Gogotsi, *Adv. Mater.* **26**, 992 (2014).
 - [13] S. Manzeli, D. Ovchinnikov, D. Pasquier, O. V. Yazyev, and A. Kis, *Nat. Rev. Mater.* **2**, 17033 (2017).
 - [14] W. Zhang, R. Yu, H.-J. Zhang, X. Dai, and Z. Fang, *New J. Phys.* **12**, 065013 (2010).
 - [15] M. Wuttig and N. Yamada, *Nat. Mater.* **6**, 824 (2007).
 - [16] A. Pirovano, A. L. Lacaita, A. Benvenuti, F. Pellizzer, and R. Bez, *IEEE Trans. Electron Devices* **51**, 452 (2004).
 - [17] R. Simpson, P. Fons, A. Kolobov, T. Fukaya, M. Krbal, T. Yagi, and J. Tominaga, *Nat. Nanotechnol.* **6**, 501 (2011).
 - [18] A. Koma, *Thin Solid Films* **216**, 72 (1992).
 - [19] Y. Shi, W. Zhou, A.-Y. Lu, W. Fang, Y.-H. Lee, A. L. Hsu, S. M. Kim, K. K. Kim, H. Y. Yang, L.-J. Li *et al.*, *Nano Lett.* **12**, 2784 (2012).

- [20] G. Binnig, H. Rohrer, C. Gerber, and E. Weibel, *Phys. Rev. Lett.* **50**, 120 (1983).
- [21] W. Mönch, *Semiconductor Surfaces and Interfaces* (Springer Science & Business Media, New York, 2013), Vol. 26.
- [22] J. Momand, J. E. Boschker, R. Wang, R. Calarco, and B. J. Kooi, *Cryst. Eng. Comm.* **20**, 340 (2018).
- [23] R. Wang, F. R. Lange, S. Cecchi, M. Hanke, M. Wuttig, and R. Calarco, *Adv. Funct. Mater.* **28**, 1705901 (2018).
- [24] S. Cecchi, D. Dragoni, D. Kriegner, E. Tisbi, E. Zallo, F. Arciprete, V. Holy, M. Bernasconi, and R. Calarco, *Adv. Funct. Mater.* **29**, 1805184 (2019).
- [25] E. Zallo, D. Dragoni, Y. Zaytseva, S. Cecchi, N. I. Borgardt, M. Bernasconi, and R. Calarco, *Phys. Status Solidi (RRL)* **15**, 2000434 (2021).
- [26] R. Wang, V. Bragaglia, J. E. Boschker, and R. Calarco, *Cryst. Growth Des.* **16**, 3596 (2016).
- [27] S. Borisova, J. Krumrain, M. Luysberg, G. Mussler, and D. Grützmacher, *Cryst. Growth Des.* **12**, 6098 (2012).
- [28] F. Lüpke, S. Just, G. Bihlmayer, M. Lanius, M. Luysberg, J. c. v. Doležal, E. Neumann, V. Cherepanov, I. Ošťádal, G. Mussler, D. Grützmacher, and B. Voigtländer, *Phys. Rev. B* **96**, 035301 (2017).
- [29] H. B. Elswijk, D. Dijkamp, and E. J. van Loenen, *Phys. Rev. B* **44**, 3802 (1991).
- [30] S. Bengió, M. Martin, J. Avila, M. C. Asensio, and H. Ascolani, *Phys. Rev. B* **65**, 205326 (2002).
- [31] P. Giannozzi, S. Baroni, N. Bonini, M. Calandra, R. Car, C. Cavazzoni, D. Ceresoli, G. L. Chiarotti, M. Cococcioni, I. Dabo *et al.*, *J. Phys.: Condens. Matter* **21**, 395502 (2009).
- [32] N. Troullier and J. L. Martins, *Phys. Rev. B* **43**, 1993 (1991).
- [33] J. P. Perdew, K. Burke, and M. Ernzerhof, *Phys. Rev. Lett.* **77**, 3865 (1996).
- [34] S. Grimme, *J. Comput. Chem.* **27**, 1787 (2006).
- [35] H. J. Monkhorst and J. D. Pack, *Phys. Rev. B* **13**, 5188 (1976).
- [36] N. Marzari, D. Vanderbilt, A. De Vita, and M. C. Payne, *Phys. Rev. Lett.* **82**, 3296 (1999).
- [37] H. J. Berendsen, J. v. Postma, W. F. van Gunsteren, A. DiNola, and J. R. Haak, *J. Chem. Phys.* **81**, 3684 (1984).
- [38] P. Becker, K. Dorenwendt, G. Ebeling, R. Lauer, W. Lucas, R. Probst, H.-J. Rademacher, G. Reim, P. Seyfried, and H. Siegart, *Phys. Rev. Lett.* **46**, 1540 (1981).
- [39] R. R. Reeber and K. Wang, *Mater. Chem. Phys.* **46**, 259 (1996).
- [40] A. Jain, S. P. Ong, G. Hautier, W. Chen, W. D. Richards, S. Dacek, S. Cholia, D. Gunter, D. Skinner, G. Ceder, and K. A. Persson, *APL Mater.* **1**, 011002 (2013).
- [41] J. Akola and R. O. Jones, *Phys. Rev. B* **85**, 134103 (2012).
- [42] T. H. Lee and S. R. Elliott, *Adv. Mater.* **29**, 1700814 (2017).
- [43] D. Dragoni and M. Bernasconi, *J. Chem. Phys.* **151**, 134503 (2019).
- [44] W. Hume-Rothery, *London, Edinburgh, and Dublin Phil. Mag. J. Sci.* **9**, 65 (1930).
- [45] P. Grosse and K. Winzer, *Phys. Status Solidi B* **26**, 139 (1968).
- [46] F. Kirchhoff, N. Binggeli, G. Galli, and S. Massidda, *Phys. Rev. B* **50**, 9063 (1994).
- [47] G. Sosso, S. Caravati, and M. Bernasconi, *J. Phys.: Condens. Matter* **21**, 095410 (2009).
- [48] R. Keller, W. B. Holzapfel, and H. Schulz, *Phys. Rev. B* **16**, 4404 (1977).
- [49] See Supplemental Material at <http://link.aps.org/supplemental/10.1103/PhysRevB.106.195427> for additional information on the structural and electronic properties of the models considered in this paper.
- [50] A sg15 optimized norm-conserving Vanderbilt (oncv) pseudopotential [54] for silicon has been used for the calculation of the DOS.
- [51] J. Pendry, K. Heinz, W. Oed, H. Landskron, K. Müller, and G. Schmidlein, *Surf. Sci.* **193**, L1 (1988).
- [52] Secondary superstructures of minor intensity would add up only in case of presence of correlated atomic displacements [55].
- [53] B. Powell and P. Martel, *J. Phys. Chem. Solids* **36**, 1287 (1975).
- [54] D. R. Hamann, *Phys. Rev. B* **88**, 085117 (2013).
- [55] P. B. Moore, *Structure* **17**, 1307 (2009).